Supporting Information

S1 Characterization of α -FeOOH

SEM images in Fig. S1 revealed the rod shape or needle-like of α-FeOOH catalyst as reported in literature (Sahu et al., 2016; Sun et al., 2018).

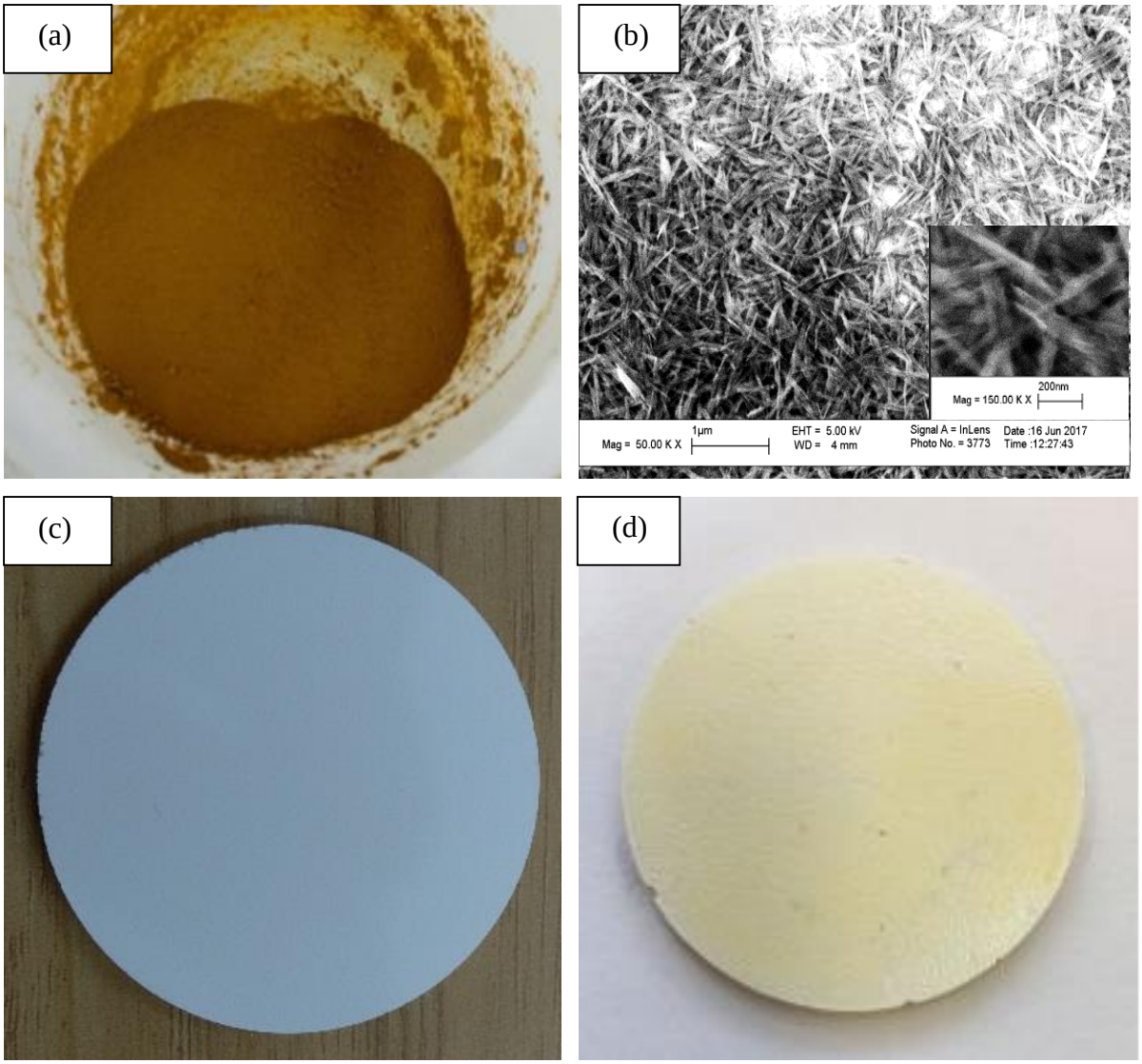

Fig. S1 Photo (a) and SEM images (b) of α-FeOOH catalyst; (c) and (d) are photos of uncoated and coated membrane

S2 Schematic of the batch experiment of Photo-Fenton degradation

Figure S2 shows the apparatus of batch experiment.

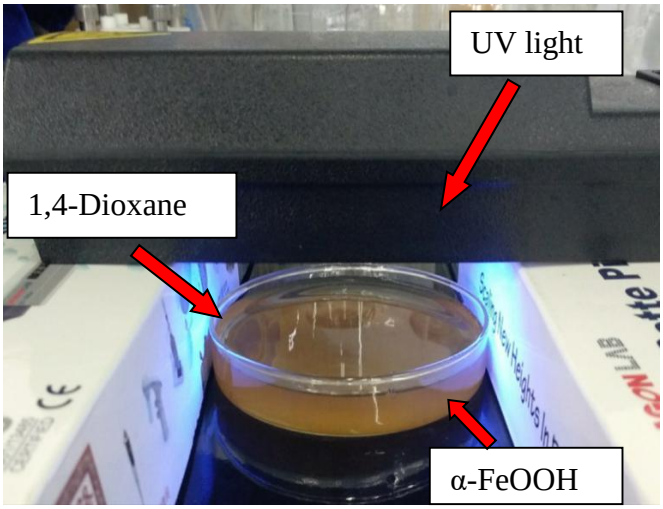

Fig. S2 Schematic of the batch experiment of Photo-Fenton degradation

S3 Control of influent flux and pollutant loading

The photogenerated electron transfer rate (J_P) and the electron loading rate or electron flux (J_e) calculated by the method we reported elsewhere (Sun et al., 2020). The key parameters we used in the calculation include: 1) The hypothetical quantum yield (η), which is assumed to be 10% ±5%; 2) the UV intensity: 2000 μW/cm^2; 3) The effective UV-exposure area on the membrane surface: 13.20 cm^2; 4) the band gap of α-FeOOH catalyst: 2.5 eV; 5) the influent concentration of 1,4-Dioxane (0.11 mmol/L); and 6) the number of the total electrons in each 1,4-Dioxane molecule (n): 4 e$^-$. The rate of photogenerated electrons (J_P) should be greater than the receiving electron loading rate from the influent (J_e), which results in the relationship of the influent flow rate (Q) and the 1,4-Dioxane concentration (C) under hypothetical quantum yields (η) in Fig. S3. If the initial 1,4-Dioxane concentration increases, the influent flow rate (Q) should be reduced accordingly to meet $Q = \frac{J_e}{nC_{1,4-Dioxane}} \le \frac{J_P}{nC_{1,4-Dioxane}}$ to achieve a complete photochemical oxidation of 1,4-Dioxane during the photocatalytic membrane filtration. Likewise, with higher quantum yields, the allowable influent flow rate could be greater due to higher rates of photogenerated electron transfer.

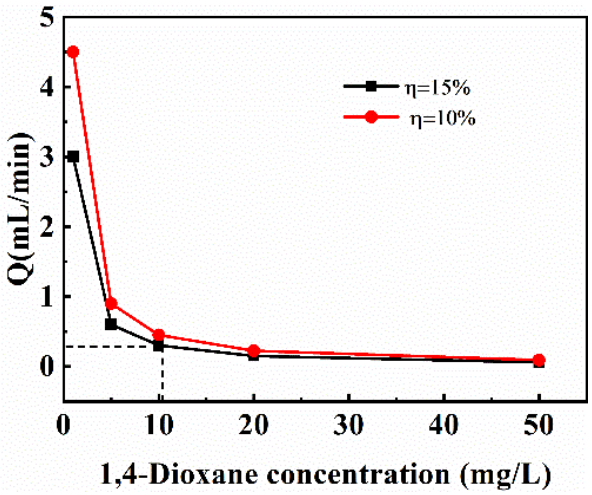

Fig. S3 The maximum allowed influent flow rate (Q) at 1,4-Dioxane concentration (i.e., C values) of 1,4-Dioxane at different hypothetical levels of quantum yield (i.e., η values)

S4 Calculation for AQY

The # of 1,4-Dioxane degraded per time can be calculated by Eq. (S1):

$$\#\text{of 1,4-Dioxane degraded per time} = \frac{\Delta c \cdot V \cdot \mathrm{n}}{t \cdot M} \quad , \qquad \text{(S1)}$$

where Δc is the remaining concentration of 1,4-Dioxane at a reaction time *t*. It can be estimated from Fig. S4, t is the reaction time, 7200 s. Δc were 2.77 mg/L and 8.38 mg/L when UV wavelengths were 365 nm and 254 nm, respectively. n is electron donor number of each 1,4-Dioxane molecule (e^-/mol), 20 e^-/mol; V is the volume of solution, 60 mL; M is molar mass of the 1,4-Dioxane, 88 g/mol. Therefore, the # of 1,4-Dioxane degraded per time for 365 nm and 254 nm were 5.25×10^{-9} e^-/s and 1.59×10^{-8} e^-/s, respectively.

The photon radiance E_{QF} (# of UV photons per time) was measured at 365 nm or 254 nm, which was calculated according to Eq. (S2):

$$E_{QF} = \frac{N_P}{N_A} \quad , \qquad \text{(S2)}$$

where N_A is the Avogadro's number (6.02×10^{23}). N_p is the number of photons per second and per surface unit (#photon/(cm^2·s)), the UV-irradiated area of 13.2 cm^2 as mentioned above. N_P was calculated by Eq. (S3):

$$N_P = \frac{I}{E_P} \quad , \qquad \text{(S3)}$$

where I is the incident light intensity, light intensities are 2000 μw/cm^2 and 401 μw/cm^2 when the UV wavelength are 365 nm and 254 nm. A photon at a certain wavelength has an energy (Ep) that can be calculated according to Eq. (S4):

$$E_P = \frac{hc}{\lambda} \quad , \qquad \text{(S4)}$$

where h is the Planck constant (6.626×10^{-34} J s), c is the light speed (3×10^{8} m/s), λ is the light wavelength (365 nm / 254 nm).

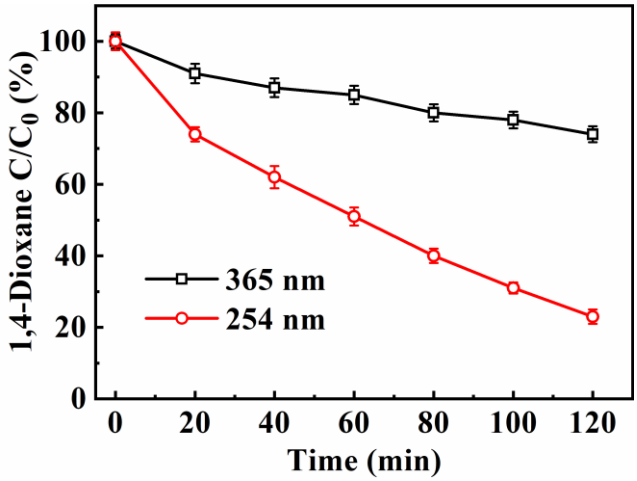

Fig. S4 The ratio of the residual concentration (C) to the initial concentration (C_0) of 1,4-Dioxane under different UV wavelength. Initial 1,4-Dioxane concentration: 10.8 mg/L; H_2O_2 concentration: 2 mmol/L; and the catalyst dosage: 1 g/L

S5 Comparison of •OH generated under different reaction condition

The fluorescence spectra of different reaction conditions Fig. S5 shows that he •OH production followed by the order of: H_2O_2/UV > H_2O_2/UV/α-FeOOH > α-FeOOH/ H_2O_2 > α-FeOOH/UV > α-FeOOH > H_2O_2 > UV.

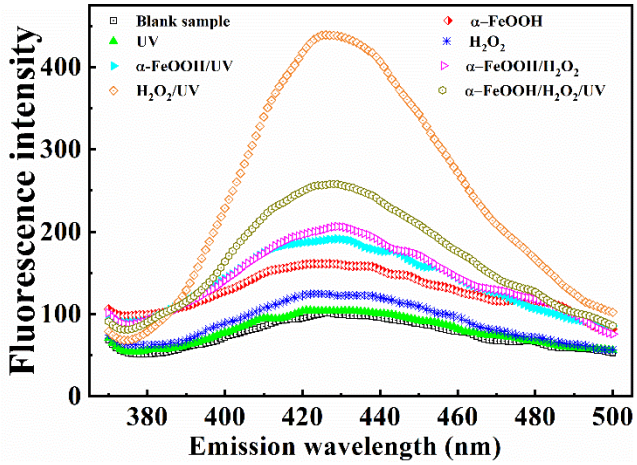

Fig. S5 Comparison of •OH generated under different reaction condition. 1,4-Dioxane concentration: 10.8 mg/L; α-FeOOH: 1 g/L; and H_2O_2 concentration: 2 mmol/L

S6 Mechanisms of 1,4-Dioxane degradation in different heterogeneous photo-Fenton systems

Table S1 Mechanisms of 1,4-Dioxane degradation in different heterogeneous photo-Fenton system

Catalysis	Degradation pathways and mechanisms
WO_3/nγ-Al_2O_3 (Xu et al., 2019)	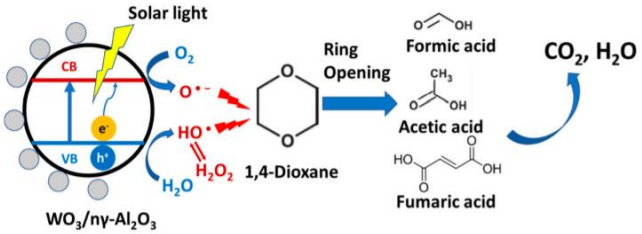 HO• and $O_2^{\bullet-}$/$HO_2^{\bullet}$ radicals were produced by WO_3/nγ-Al_2O_3-based photocatalytic system and degraded 1,4-Dioxane.
Zero valent iron (Fe^0) microsphere (Barndők et al., 2016a)	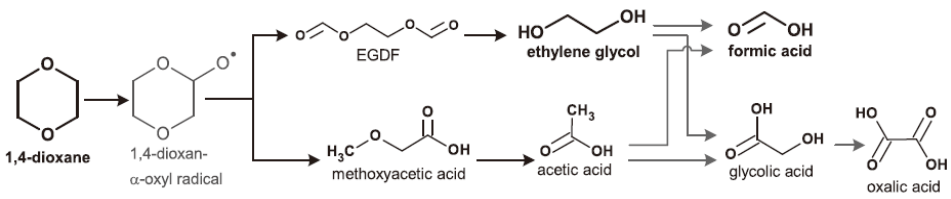 •OH produced from photo-Fenton system in which Fe^0 as an effective catalyst. The primary intermediates were Ethylene glycol and formic acid in heterogeneous photo-Fenton.

Clay minerals (Zeng et al., 2017)

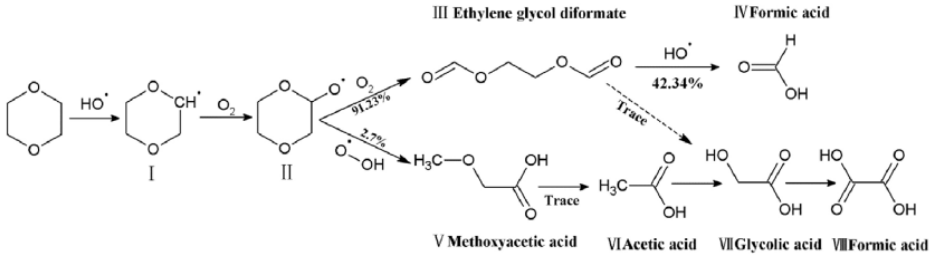

•OH was generated by structural Fe(II) oxygenation in ferruginous clay minerals. There are two possible pathways for the degradation of the α-oxyl radical.

NF-TiO_2 (Barndõk et al., 2016b)

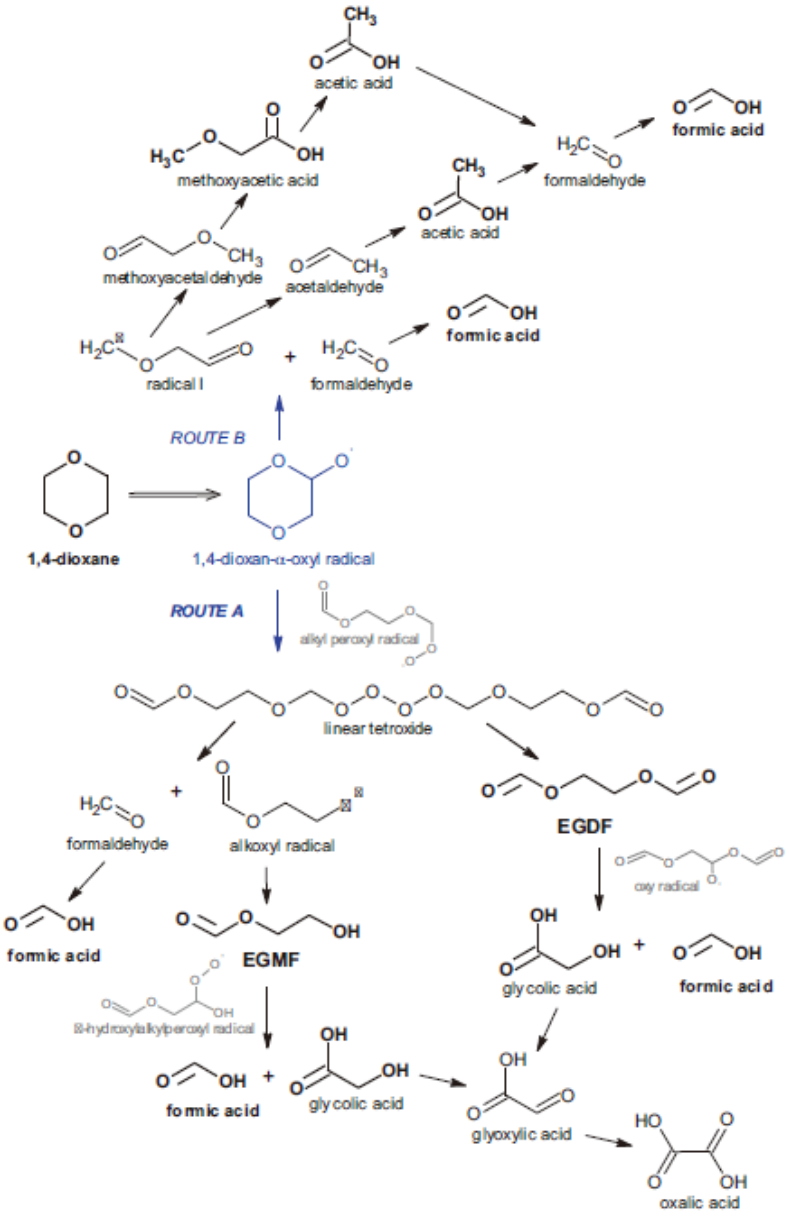

•OH or •O_2^- produced from solar photocatalysis system using immobilized NF-TiO_2 composite with monodisperse TiO_2 nanoparticles. According to the literature, EGDF and EGMF are produced in an oxidative ring opening mechanism .This α-oxyl radical can be degraded either through the route A or through an intramolecular reaction followed by fragmentation (route B).

S7 Optimal structures of the reactant, transformation products and intermediates

Table S2 Optimal structures of the reactant (R), transformation products (TP) and intermediates (IM)

Name	Structure
1,4-Dioxane (R)	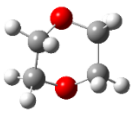
Dioxanyl radicals (IM_1)	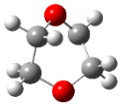
Peroxyl radicals (IM_2)	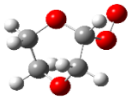
1,4-Dioxane-α-oxyl radical (IM_3)	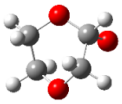
Ethylene glycol diformate (TP_1)	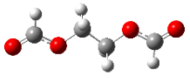
Yield ethylene glycol (TP_2)	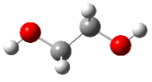
Formic acid (TP_3)	

Notes: Dark gray: C; Red: O; Light gray: H

References

Barndõk H, Blanco L, Hermosilla D, Blanco Á (2016a). Heterogeneous photo-Fenton processes using zero valent iron microspheres for the treatment of wastewaters contaminated with 1, 4-dioxane. Chemical Engineering Journal, 284: 112–121

Barndõk H, Hermosilla D, Han C, Dionysiou D D, Negro C, Blanco Á (2016b). Degradation of 1, 4-dioxane from industrial wastewater by solar photocatalysis using immobilized NF-TiO_2 composite with monodisperse TiO_2 nanoparticles. Applied Catalysis B: Environmental, 180: 44–52

Sahu R, Song B J, Jeon Y P, Lee C W (2016). Upgrading of vacuum residue in batch type reactor using Ni–Mo supported on goethite catalyst. Journal of Industrial and Engineering Chemistry, 35: 115–122

Sun S, Yao H, Fu W, Hua L, Zhang G, Zhang W (2018). Reactive Photo-Fenton ceramic membranes: Synthesis, characterization and antifouling performance. Water Research, 144: 690–698

Sun S, Yao H, Fu W, Xue S, Zhang W (2020). Enhanced degradation of antibiotics by photo-fenton reactive membrane filtration. Journal of Hazardous Materials, 386: 121955

Xu X, Liu S, Cui Y, Wang X, Smith K, Wang Y (2019). Solar-driven removal of 1, 4-Dioxane using WO_3/nγ-Al_2O_3 nano-catalyst in water. Catalysts, 9(4): 389

Zeng Q, Dong H, Wang X, Yu T, Cui W (2017). Degradation of 1, 4-dioxane by hydroxyl radicals produced from clay minerals. Journal of Hazardous Materials, 331: 88–98